Memoirs of the Faculty of Engineering, Nagoya University
Vol. 41, No. 2 (1989) –Research Report–

EXPERIMENTS ON TURBULENT FLOW IN A SQUARE DUCT WITH A ROUGH WALL

HIDEOMI FUJITA, MASAFUMI HIROTA
and HAJIME YOKOSAWA*

Department of Mechanical Engineering

(Received October 31, 1989)

Abstract

The purpose of this experimental study is to make clear the characteristics of a fully developed turbulent flow in a square duct with the bottom wall rough and the remaining walls smooth. Detailed and reliable results have been obtained by hot-wire anemometry for such quantities as primary flow velocity, secondary flow velocities, turbulence intensities, and turbulent shear stresses.

A pattern of secondary flow very different from those reported until now has been found in the rough duct: only two large, contra-rotating longitudinal vortices have appeared in any given cross-section. Moreover, not only anisotropy of normal stresses ($\overline{u_2^2}-\overline{u_3^2}$) but also turbulent shear stress $\overline{u_2u_3}$ in the rough duct has been found to be an important contributor to the generation of the secondary flow of Prandtl's second kind.

Notation

B	half length of a side of square duct
D	hydraulic diameter or a side of square duct$=2B$
k	kinetic energy of turbulence
P	mean static pressure
Re	Reynolds number based on U and D $(=U\cdot D/\nu)$
U	bulk mean velocity

* College of General Education, Nagoya University

U_1, U_2, and U_3 components of mean velocity in each coordinate direction
U_S maximum of mean axial velocity
u_1, u_2, and u_3 components of fluctuating velocity in each coordinate direction
X_1, X_2, and X_3 orthogonal coordinates (defined in Fig. 2)
λ resistance coefficient of the rough duct
ρ density of fluid
τ_w wall shear stress
ν kinematic viscosity of fluid
Ω mean vorticity vector

1. Introduction

Secondary flow of Prandtl's second kind[1] is one of the most characteristic phenomena observed in turbulent flows through non-circular straight ducts[2),3)]. It is well known that a smooth walled duct yields eight cells of streamwise vortices in its cross-section. Although velocities of the secondary flow amount to at most several percent of the maximum primary flow velocity, the secondary flow has a great influence on flow and temperature fields[4)-6)]. The behavior and the origin of the secondary flow of the second kind have attracted the interest of many investigators, and numerous studies have been reported in connection with the flow, especially with that in smooth-walled square ducts[7)-12)].

The origin of the secondary flow of the second kind lies in the anisotropy of the turbulent stress fields. If turbulent stress fields are altered by roughening some of the walls forming non-circular ducts, the secondary flow patterns in the ducts would most likely change. Indeed Fujita found that various square ducts consisting of smooth and rough planes have their own peculiar distortions in the contour lines of the primary flow velocity[13)]. In order to make clear the influences of rough walls on the generation of the secondary flow of the second kind, it is indispensable to accumulate detailed data of velocity and stress fields in various rough ducts. However, to the authors' knowledge, very few reports to date have dealt with such a complicated flow field as found in the rough ducts [14),15)]. One of the most detailed experimental studies was done by Humphrey and Whitelaw[16)], but they presented only one component of the two transverse velocities. Therefore, the reason for the changes in the secondary flow pattern and turbulent stress fields caused by the existence of the rough wall has not yet been entirely clarified. With this in mind, the authors have conducted detailed measurements and numerical analyses of turbulent flows through several kinds of rectangular ducts with rough walls. The results reflect extremely different patterns of secondary flow appearing in these ducts in response to their own turbulent stress fields altered by the rough walls[17)-19)].

In this report, at first, detailed and comprehensive results are shown from measurements in a fully developed turbulent flow through a square duct with one rough wall. Next, by evaluating each term of a vorticity transport equation, we discuss the cause of the generation of the secondary flow, and investigate in detail the applicability to the rough duct of conventional theories, which have been derived from the results obtained in smooth walled ducts.

2. Experiment

The schema of the present flow apparatus shown in Fig. 1 is essentially the same as that used in the prior experiment on a square duct with roughened walls[19]. Air is supplied by a centrifugal fan to the test duct through an exactly calibrated quadrant flow nozzle and a settling chamber. The test duct is straight, with a square cross-section of 50×50 mm, measures 4500 mm in length, and is made of smooth transparent acrylic resin plates.

Brass roughness elements with a cross-section of 1 mm square are glued to the bottom wall orthogonally to the primary flow direction over the entire length of the duct, as shown in Fig. 2. Roughness elements are set up at an interval of 10 mm, i.e., pitch to height ratio is 10:1, so that the flow resistance is largest. A resistance coefficient of this duct λ obtained in the present experiment is formulated empirically as follows for $2\times10^4<Re<9\times10^4$.

$$\lambda=2D(-dP/dX_1)/\rho U^2=0.161Re^{-0.138} \tag{1}$$

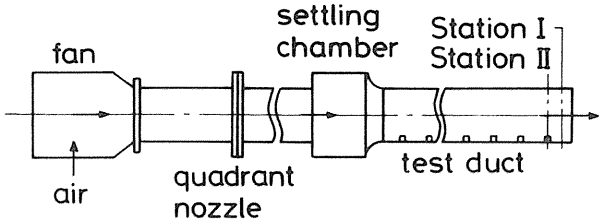

Fig. 1. Experimental apparatus

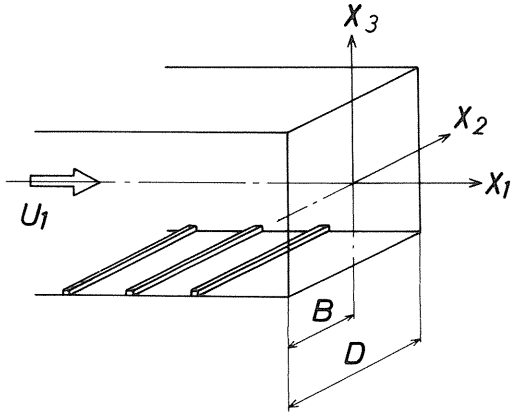

Fig. 2. Coordinate system

As shown in Fig. 2, the X_1-axis is along the duct centerline, X_2- and X_3-axes are orthogonal coordinates in the lateral cross-section. Each component of mean velocity is denoted by U_1, U_2 and U_3, and that of fluctuating velocity u_1, u_2 and u_3.

Measurements were conducted in the smooth duct as well as in the rough one, keeping Reynolds number Re at 6.5×10^4. Two types of hot-wire probes, normal and X-wire types, were used in measuring the mean velocity components and the turbulent stresses. A novel technique involving the use of two X-wire probes[20] was applied to measure transverse velocity components accurately. The measurements were performed mainly at the cross-section which was located 5 mm downstream from the roughness element furthest downstream, i.e., $89.6D$ downstream from a duct inlet (Station I in Fig. 1). Measurements in the smooth duct were also performed at the same station. In both ducts the primary flow velocity at the center of the cross-section does not change axially when the axial distance from the duct inlet exceeds $50D$. Therefore, flows in both ducts can be regarded as a fully developed flow at measuring stations in a global sense. The number of measuring positions over an entire cross-section was about 1000. The traversing pitch of probes was set finer as the wall was approached.

In addition to the distributions of the quantities described above over the duct cross-section, local wall shear stresses on the smooth walls were measured by the Preston tube of 1 mm in o.d. and 0.8 mm in i.d., and calculated with Patel's equation[21].

3. Results and Discussion

In both the smooth and rough ducts, experimental results on turbulence properties as well as mean flow velocities exhibited excellent symmetry with respect to the planes of symmetry of ducts, as clearly recognized from Fig. 4. Therefore, the authors show the results obtained in the half of a cross-section mainly in contour maps. The broken line drawn at the bottom of each figure for the rough duct shows the height of a roughness element. The numbers in the figures represent the values normalized by the maximum primary velocity U_S.

The uncertainties involved in measured values were estimated for the rough duct as follows[22]: U_1: $\pm1.4\,\%$, U_2 and U_3: $\pm6.0\,\%$, $\overline{u_1^2}$: $\pm2.4\,\%$, $\overline{u_2^2}$: $\pm8.3\,\%$, $\overline{u_3^2}$: $\pm8.9\,\%$, $\overline{u_1u_2}$: $\pm5.6\,\%$, and $\overline{u_1u_3}$: $\pm4.2\,\%$.

3. 1. *Wall Shear Stress*

The Preston tube method used here to measure τ_w is valid only in the flow field in which the distribution of the primary flow velocity is described by the logarithmic law. Thus, in the present experiment, the authors ascertained that the logarithmic law was valid for the primary flow velocity distributions over the smooth walls of the rough duct as well as those of the smooth duct.

Figure 3 shows the distributions of the wall shear stress τ_w measured on each smooth wall of the rough duct and the smooth duct. $\overline{\tau_w}$ designates the integral mean of τ_w obtained on each wall. On the top smooth wall opposite to the rough wall, the distribution profile of $\tau_w/\overline{\tau_w}$ of the rough duct is qualitatively similar to that of the smooth duct. That is, it shows the local minimum at $X_2/B=0$ (the wall bisector), and the maximum at $X_2/B\fallingdotseq\pm0.5$ (midway between the wall bisector and the adjacent wall). The difference between the local minimum and the maximum of $\tau_w/\overline{\tau_w}$ in the rough duct is, however, quite larger than that of the smooth duct. On the other hand, in the distribution

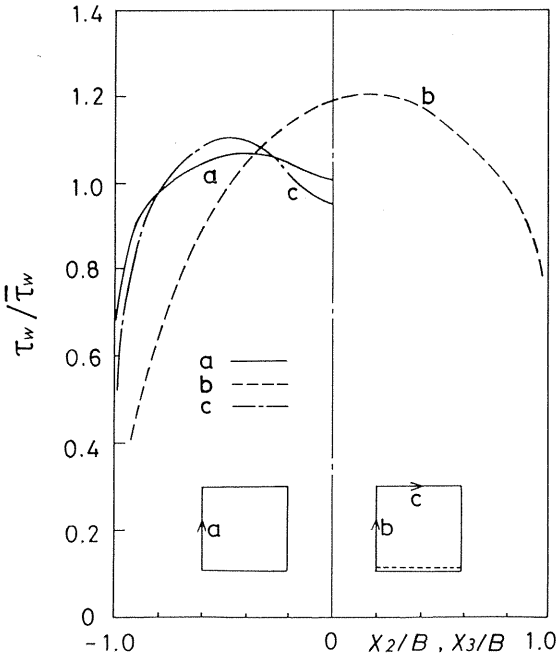

Fig. 3. Wall shear stress distributions on smooth walls

obtained on the smooth wall adjacent to the rough wall, no local minimum appears and $\tau_w/\overline{\tau_w}$ attains to the maximum at $X_3/B \fallingdotseq 0.2$. Such features of τ_w distributions as described above are closely related to the U_1 distribution shown in the following section.

The value of $\overline{\tau_w}$ on the rough wall was estimated using the method described in Ref. (13). It was so large as to attain to 50–60 % of the total flow resistance of the rough duct.

3. 2. *Primary Flow Velocity*

Figure 4 is a contour map of the primary flow velocities U_1. As has been reported, the contours in the smooth duct are distorted toward the corners of the duct owing to the corner-oriented secondary current. In the rough duct, however, the contour map is quite different from that for the smooth duct. The contours near the top smooth wall have great concavities toward the center of the cross-section, and those near the bottom rough wall are almost parallel to the wall. On the other hand, the contours near the side wall are apparently curved outward. The concavities of the contours observed near the top wall have already been reported by Humphrey and Whitelaw[16], who measured a turbulent flow in a square duct with larger roughness elements than ours using a laser-Doppler anemometer (LDA). However, the outward curve of the contours observed near the side wall in the present experiment has not been found in their duct.

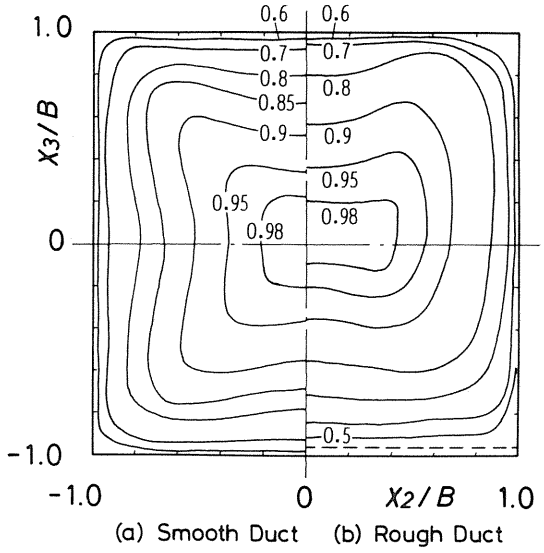

Fig. 4. Axial mean velocity U_1/U_S

3. 3. *Secondary Flow Vectors*

Figure 5 shows the secondary flow vectors in the rough duct, which were obtained from the measured transverse velocities U_2 and U_3. In general, the exact measurement of the secondary currents is quite difficult. Nevertheless, in the present experiment, a reliable secondary flow pattern was obtained as shown in Fig. 5, in which the symmetry with respect to the plane $X_2=0$ is excellent.

It is well known that a smooth square duct yields eight cells of secondary flow vortices[10]. The secondary flow pattern in the rough duct is remarkably different from that in the smooth duct. In the rough duct, secondary currents proceed from the top smooth wall toward the bottom rough wall along the duct midplane, and then toward the top wall along the side smooth wall via a lower corner. Therefore, in a cross-section of the rough duct, there are only two large cells of contra-rotating longitudinal vortices symmetric with respect to the plane $X_2=0$.

The form of U_1 contours shown in Fig. 4 is closely related to the secondary flow pattern. The contour lines of U_1 are curved inward by the secondary current at the area where the secondary current directs its course to the duct center, as recognized from the secondary flow vectors near the wall bisectional planes in the smooth duct. In the rough duct, the deep concavity in U_1 contours observed near the top smooth wall is also attributed to the secondary current flowing downward along the plane $X_2=0$. On the contrary, inward concavity is not found in the U_1 contours near the side smooth wall, because the secondary currents do not proceed to the duct center along the plane $X_3=0$.

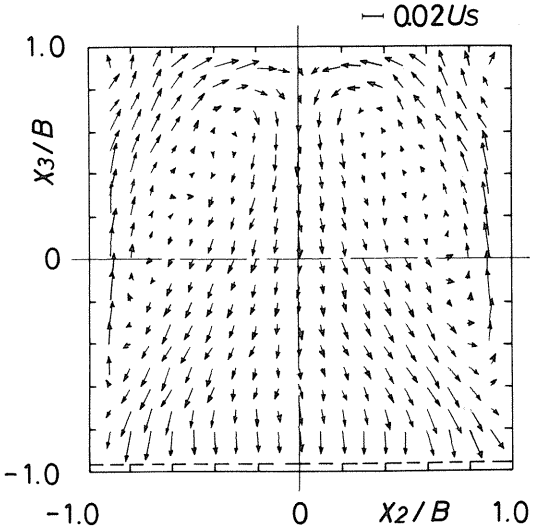

Fig. 5. Secondary flow vectors obtained at Station I

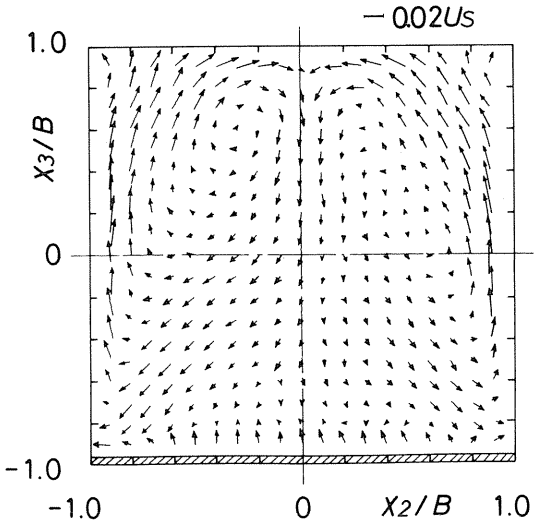

Fig. 6. Secondary flow vectors obtained at Station II

Since the rough wall was made of a smooth plate and rib roughness elements glued regularly to it, the characteristics of the flow near the rough wall vary in the X_1-direction locally, even if the flow is fully developed globally[16]. Figure 6 shows the secondary flow vectors obtained in the cross-section involving the roughness element furthest downstream (Station II, see Fig. 1). In contrast to Fig. 5 which was obtained at Station I, upward currents are observed right above the roughness element. The region where such upward currents appear is, however, limited only in a small area near the roughness element. As recognized from this result, the effects of a discrete roughness on the overall secondary flow pattern seem to be small. Nevertheless, the local variation of the flow in the X_1-direction observed near the rough wall invalidates the condition of continuity for the secondary currents in a cross-section, as seen in Fig. 5 and Fig. 6.

3. 4. Turbulence Intensities

As shown in Fig. 7, the form of contours of $\sqrt{\overline{u_1^2}}$ in the smooth duct is similar to that of U_1, shown in Fig. 4, except that the concavity of the contours toward the duct center is quite pronounced. The distribution of $\sqrt{\overline{u_1^2}}$ in the upper half section of the rough duct is qualitatively and quantitatively similar to that in the smooth duct. In the lower part, on the other hand, the level of $\sqrt{\overline{u_1^2}}$ near the rough wall is about two times as high as that in the smooth duct.

The contour map of $\sqrt{\overline{u_2^2}}$ shown in Fig. 8 is similar to that of $\sqrt{\overline{u_1^2}}$, but the level of $\sqrt{\overline{u_2^2}}$ is appreciably lower than that of $\sqrt{\overline{u_1^2}}$ over the entire cross-section in both the smooth and rough ducts.

In the smooth duct, contours of $\sqrt{\overline{u_3^2}}$, shown in Fig. 9, and those of $\sqrt{\overline{u_2^2}}$, are almost symmetric with respect to the diagonal planes of the duct. In the rough duct, there is also a region with large values near the rough wall with $\sqrt{\overline{u_3^2}}$ distribution similar to $\sqrt{\overline{u_1^2}}$ and $\sqrt{\overline{u_2^2}}$. Near the side walls, the distribution of $\sqrt{\overline{u_3^2}}$ is markedly different from that of $\sqrt{\overline{u_2^2}}$. Thus, the values of $\sqrt{\overline{u_3^2}}$ are quite large near the side smooth walls as well as near the rough wall. Since the side wall restrains the movement of fluid particles in the X_2-direction, the values of $\sqrt{\overline{u_2^2}}$ near the side wall are smaller than those of $\sqrt{\overline{u_3^2}}$. However, in the remaining area of the cross-section, the values of $\sqrt{\overline{u_2^2}}$ are considerably larger than those of $\sqrt{\overline{u_3^2}}$.

Contours of the turbulent kinetic energy $k=(\overline{u_1^2}+\overline{u_2^2}+\overline{u_3^2})/2$ in Fig. 10 are, as expected from its definition, quite similar to those of turbulence intensities. Its value near the rough wall is about three times as large as the maximum in the smooth duct. However, the minimum of k in the rough duct observed on the duct midplane at $X_3/B \fallingdotseq 0.15$ is almost the same as in the smooth duct.

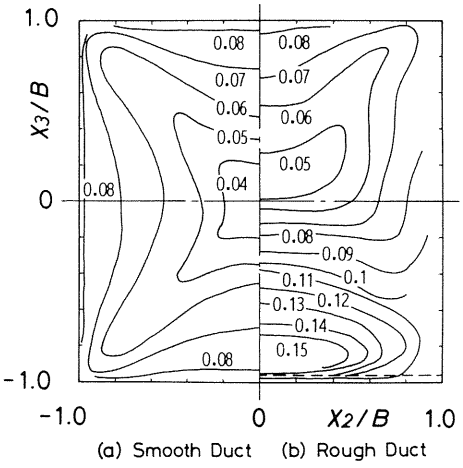

Fig. 7. Component of fluctuating velocity in the X_1-direction $\sqrt{\overline{u_1^2}}/U_S$

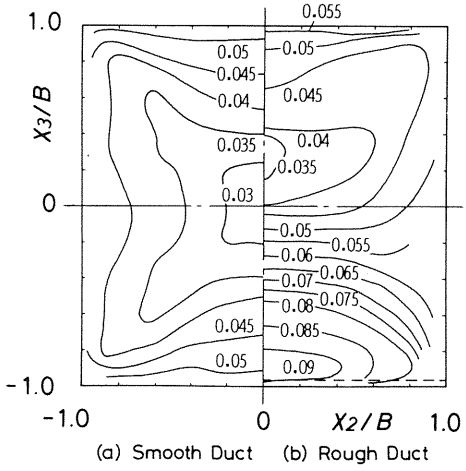

Fig. 8. Component of fluctuating velocity in the X_2-direction $\sqrt{\overline{u_2^2}}/U_S$

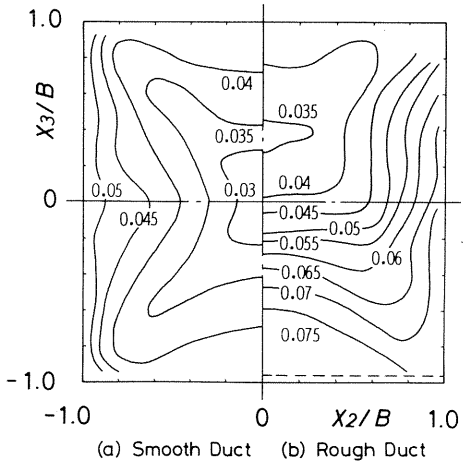

Fig. 9. Component of fluctuating velocity in the X_3-direction $\sqrt{\overline{u_3^2}}/U_S$

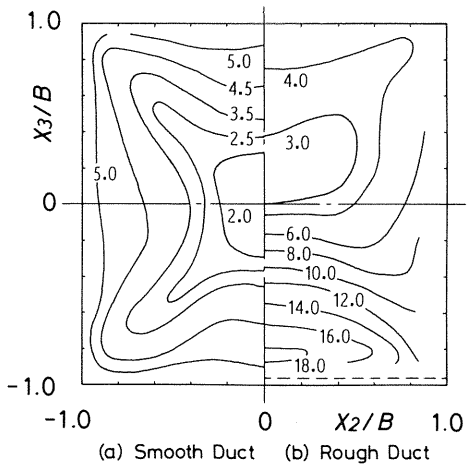

Fig. 10. Turbulent kinetic energy $k/U_S^2 \times 10^3$

3. 5. *Turbulent Shear Stresses*

Figure 11 shows the contours of $\overline{u_1u_2}$. In the smooth duct, there are closed contours enclosed by a contour for $\overline{u_1u_2}=0$ near the top and the bottom walls. This contour map is almost the same as that reported by Melling and Whitelaw[10]. Although the distribution of $\overline{u_1u_2}$ in the rough duct is qualitatively similar to that in the smooth duct, some quantitative difference is found between the two. The absolute values for the contours in a region of closed contours observed near the top smooth wall of the rough duct are noticeably higher than those in the smooth duct. In contrast to this, the level in another region of closed contours observed near a midpoint of the rough wall is very low. Near the side smooth wall, the values in the rough duct are almost the same as those in the smooth duct.

Contours of $\overline{u_1u_3}$ in the smooth duct shown in Fig. 12 (a) are almost symmetrical in relation to those of $\overline{u_1u_2}$ in Fig. 11 (a) with respect to the diagonal planes. This shows that the results of turbulent shear stresses in this experiment are highly reliable. In the rough duct, the contour map of $\overline{u_1u_3}$ is quite different from that in the smooth duct. The values of $\overline{u_1u_3}$ near the rough wall are about three times those in the smooth duct. Moreover, near the side smooth wall of the present rough duct, there is no region with closed contours enclosed by the contour for $\overline{u_1u_3}=0$, which appeared in the smooth duct.

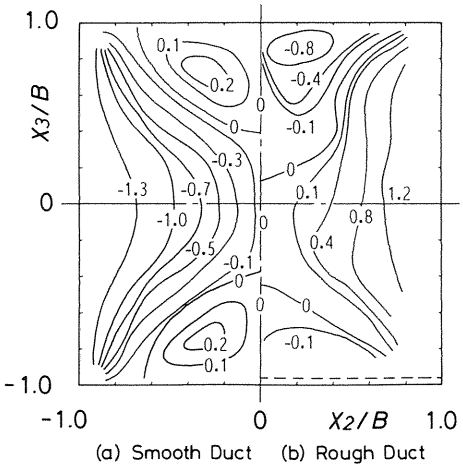

Fig. 11. Turbulent shear stress $\overline{u_1u_2}/U_S^2\times10^3$

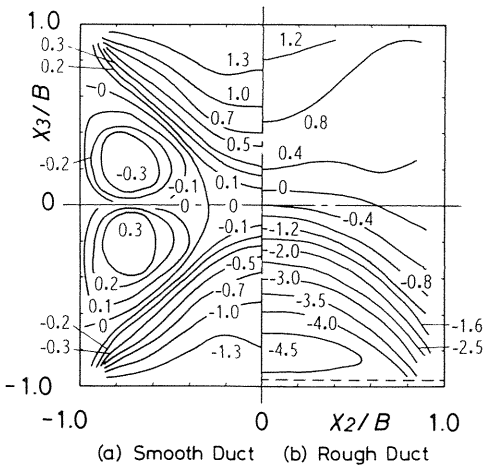

Fig. 12. Turbulent shear stress $\overline{u_1u_3}/U_S^2\times10^3$

In general, the transport of turbulent shear stress is brought about by a gradient-type diffusion caused by small-scale turbulence and by a convection caused by large-scale motions such as secondary currents. If the transport caused by small-scale eddies, namely by gradient diffusion, is dominant, turbulent shear stresses $\overline{u_1u_2}$ and $\overline{u_1u_3}$ are expressed by the mean rate of strain $\partial U_1/\partial X_2$ and $\partial U_1/\partial X_3$ as follows[23].

$$\overline{u_1u_2}=-\nu_t\partial U_1/\partial X_2,\qquad \overline{u_1u_3}=-\nu_t\partial U_1/\partial X_3 \tag{2}$$

where ν_t designates eddy viscosity, and its value may change spatially. The existence of regions of closed contours observed in Figs. 11 and 12 can be explained qualitatively by evaluating equation (2).

Figure 13 compares $\overline{u_1u_2}$ and $\partial U_1/\partial X_2$ obtained in the plane $X_3/B=0.8$ of smooth and rough ducts. In the smooth duct, $\overline{u_1u_2}$ is zero at $X_2/B=0$, a positive value at $-0.64<X_2/B<0$, zero at $X_2/B=-0.64$, and a negative value in $X_2/B<-0.64$. Therefore, in the plane $X_3/B=0.8$ of the smooth duct, the closed contours are formed in $-0.64<X_2/B<0$. On the other hand, owing to the inward curve of U_1 contours shown in Fig. 4 (a), $\partial U_1/\partial X_2$ in the smooth duct also attains zero at $X_2/B=-0.64$, and changes its sign in a manner quite opposite to $\overline{u_1u_2}$. Therefore, the portion for negative $\partial U_1/\partial X_2$ observed in $-0.64<X_2/B<0$ corresponds to the region of closed contours in $\overline{u_1u_2}$ distribution. In the rough duct, quite a similar correspondence is also observed between $\overline{u_1u_2}$ and $\partial U_1/\partial X_2$. Furthermore, the large values of $\overline{u_1u_2}$ in the closed-contour region near the top smooth wall of the rough duct can be also explained by the large values of $\partial U_1/\partial X_2$ observed in $0<X_2/B<0.48$ of the rough duct in Fig. 13. On the other hand, in $\overline{u_1u_3}$ contours of the rough duct shown in Fig. 12 (b), there are not closed contours enclosed by the contour for $\overline{u_1u_3}=0$. This is also explained reasonably by considering the correspondence of $\overline{u_1u_3}$ with $\partial U_1/\partial X_3$ as expressed in Eq. (2).

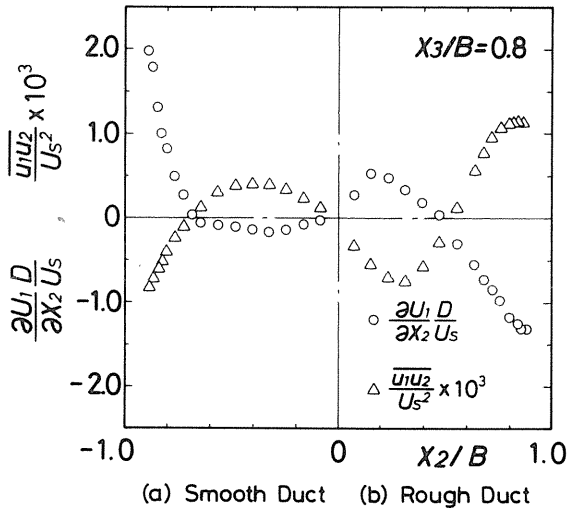

Fig. 13. Comparison between $\overline{u_1u_2}$ and $\partial U_1/\partial X_2$

As pointed out earlier, the turbulent stress model based on an isotropic eddy viscosity, namely Boussinesq's hypothesis, does not predict the generation of the secondary flow of the second kind[16]. However, as described above, the simple model based on eddy viscosity as expressed by Eq. (2) is locally effective to estimate the qualitative features of the distributions of turbulent shear stresses. This suggests that the transport of turbulent shear stresses of a flow in such a square duct as used in the present experiment may be mainly dominated by the gradient-type diffusion caused by small-scale turbulence. However, the validity of this statement should be discussed further in detail based on more extensive research.

4. Vorticity Balance

In this section, the balance between the convection and the generation of the longitudinal vorticity is examined in detail based on a vorticity transport equation. The vorticity transport equation for the X_1-component of mean vorticity $\Omega_1=\partial U_3/\partial X_2-\partial U_2/\partial X_3$ is as follows:

$$\frac{D\Omega_1}{Dt}=\nu\nabla^2\Omega_1+(\Omega\cdot\nabla)U_1+\frac{\partial}{\partial X_1}\left(\frac{\partial\overline{u_1u_2}}{\partial X_3}-\frac{\partial\overline{u_1u_3}}{\partial X_2}\right)$$
$$+\frac{\partial^2}{\partial X_2\partial X_3}(\overline{u_2^2}-\overline{u_3^2})+\left(\frac{\partial^2}{\partial X_3^2}-\frac{\partial^2}{\partial X_2^2}\right)\overline{u_2u_3} \tag{3}$$

where Ω denotes a mean vorticity vector. The secondary flow of the second kind is generated and maintained by the contribution of the third, fourth, and fifth terms on the right-hand side of Eq. (3).

From the experimental data which the authors have obtained thus far, the following results have been derived on vorticity balance for turbulent flows in several kinds of rectangular ducts.

1 For turbulent flows through smooth-walled rectangular ducts, the contribution of the fourth term on the right-hand side of Eq. (3) is almost balanced with the contribution of the convection term on the left-hand side[18]. This result is in accordance with that found by Brundrett and Baines[7] in a smooth square duct.

2 The same result in the smooth walled ducts is obtained for the square duct with two rough walls[19], in which the contribution of cross-planar normal stresses can be regarded as the most predominant for the generation of the longitudinal vortices.

3 Contrary to results described in 1 and 2, in the rectangular ducts with one rough wall, it was found that the fourth term does not necessarily balance with the convection term[18].

Figures 14 (a) and (b) show the contour maps of the convection $(U_2\partial\Omega_1/\partial X_2+U_3\partial\Omega_1/\partial X_3)$ and the production $\partial^2(\overline{u_2^2}-\overline{u_3^2})/\partial X_2\partial X_3$ obtained for the rough duct, respectively. Near the lower corner formed by the rough and smooth walls, these two terms attain the maximum values. It is also evident, however, that the convection term is not balanced with the fourth term in this region, contrary to the results obtained in the smooth duct and in the two-rough-wall duct. Hence, in the following, the contribution of other terms of vorticity transport equation is examined in detail for the present rough duct.

In the present experimental condition, the flow to be measured is fully developed in the X_1-direction. Accordingly, the vorticity transport equation, Eq. (3), can be simplified as

$$U_2\frac{\partial\Omega_1}{\partial X_2}+U_3\frac{\partial\Omega_1}{\partial X_3}=\nu\left(\frac{\partial^2\Omega_1}{\partial X_2^2}+\frac{\partial^2\Omega_1}{\partial X_3^2}\right)+\frac{\partial^2}{\partial X_2\partial X_3}(\overline{u_2^2}-\overline{u_3^2})$$
$$+\left(\frac{\partial^2}{\partial X_3^2}-\frac{\partial^2}{\partial X_2^2}\right)\overline{u_2u_3} \tag{4}$$

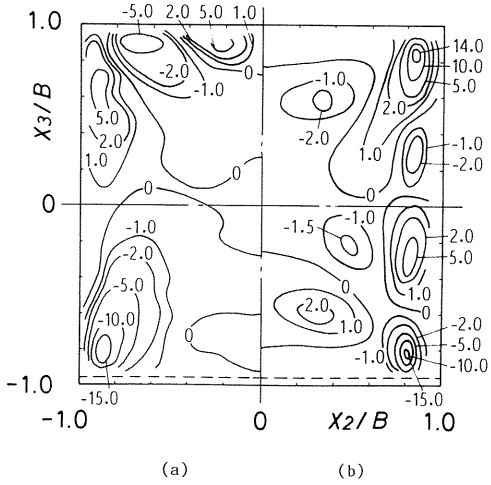

Fig. 14. (a) Convection of mean vorticity $(U_2\partial\Omega_1/\partial X_2+U_3\partial\Omega_1/\partial X_3)D^2/U_S^2\times10^2$
(b) Production of mean vorticity $(\partial^2(\overline{u_2^2}-\overline{u_3^2})/\partial X_2\partial X_3)D^2/U_S^2\times10^2$

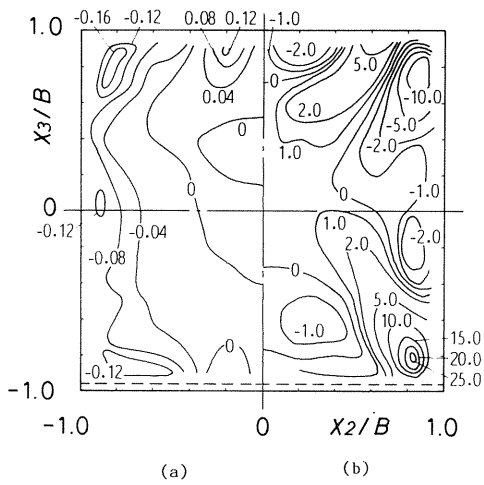

Fig. 15. (a) Convection of mean vorticity $\nu(\partial^2\Omega_1/\partial X_2^2+\partial^2\Omega_1/\partial X_3^2)D^2/U_S^2\times10^2$
(b) Production of mean vorticity $((\partial^2/\partial X_3^2-\partial^2/\partial X_2^2)\overline{u_2u_3})D^2/U_S^2\times10^2$

Equation (4) suggests that, as pointed out by Perkins[8] and Nezu and Nakagawa[24], the turbulent shear stress $\overline{u_2u_3}$ would also play an important role for the generation of the secondary flow vorticity in the rough duct. Although the behavior of the third term on the right-hand side of Eq. (4) is of much interest, an accurate measurement of $\overline{u_2u_3}$ is very difficult at the present stage[24]. Hence, the values of the first term in Eq. (4) $\nu(\partial^2/\partial X_2^2+\partial^2/\partial X_3^2)\Omega_1$, expressing the viscous diffusion of vorticity, were calculated at first, and then, the values of the third term $(\partial^2/\partial X_3^2-\partial^2/\partial X_2^2)\overline{u_2u_3}$ were obtained as a closing entry in Eq. (4). Figure 15 (a) shows the distribution of the viscous diffusion term, and Fig. 15 (b) the third term in Eq. (4) obtained for the rough duct. The viscous diffusion term attains a relatively large value near each wall. However, the level of this term is negligibly small relative to those of other terms, as shown in Fig. 14. On the other hand, the distribution of the third term shown in Fig. 15 (b) is qualitatively similar to that of the convection term shown in Fig. 14(a). If examined quantitatively, the values of the third term expressing the contribution of $\overline{u_2u_3}$ are especially large near the lower corner. In this corner region, the contribution of the shear stress $\overline{u_2u_3}$ to the generation of secondary flow vortices is almost the same as that of the cross-planar normal stresses $(\overline{u_2^2}-\overline{u_3^2})$, Fig. 14 (b), or, depending on the location, it is larger than the contribution of $(\overline{u_2^2}-\overline{u_3^2})$.

As mentioned before, in the duct with two rough walls, the contribution of $(\overline{u_2^2}-\overline{u_3^2})$ predominates for the generation of the longitudinal vortices[19]. Contrary to this, in the duct with one rough wall the contribution of $\overline{u_2u_3}$ to the generation of the longitudinal vortices is almost the same as that of $(\overline{u_2^2}-\overline{u_3^2})$. Therefore, the theory suggested by Brundrett and Baines[7] does not necessarily hold true in square ducts with rough walls. In the present rough duct, the theory proposed by Perkins[8] and Nezu and Nakagawa[24] seems to be more acceptable. Thus, the convection of mean longitudinal vorticity

$(U_2\partial\Omega_1/\partial X_2+U_3\partial\Omega_1/\partial X_3)$ is balanced with the sum of the contribution of cross-planar normal stresses $\partial^2(\overline{u_2^2}-\overline{u_3^2})/\partial X_2\partial X_3$ and that of turbulent shear stress $(\partial^2/\partial X_3^2-\partial^2/\partial X_2^2)\overline{u_2u_3}$.

5. Conclusion

The main conclusions obtained in the present experimental study are summarized as follows.

(1) The distribution of the wall shear stress on the top smooth wall of the rough duct is qualitatively similar to that of the smooth duct. On the side smooth wall, it exhibits the maximum at $X_3/B\fallingdotseq 0.2$, and the local minimum does not appear. The mean wall shear stress on the rough wall is so large as to attain to 50–60 % of the total flow resistance of the rough duct.

(2) In the rough duct there are deep concavities toward the duct center in the U_1 contours near the top smooth wall, whereas the contours are almost parallel to the wall near the rough wall, and curves outward near the side smooth walls.

(3) The secondary flow pattern in the rough duct is extremely different from that in the smooth duct. Thus, two large, contra-rotating longitudinal vortices symmetric with respect to the plane $X_2=0$ are observed in any given cross-section. Secondary currents proceed from the top smooth wall to the bottom rough wall along the plane $X_2=0$, and then return to the top wall along the side smooth wall via a lower corner.

(4) Inward curves in contours of turbulence intensities are found near the top smooth wall of the rough duct. Near the rough wall, the levels of turbulence intensities are about two times as large as those in the smooth duct. Moreover, in the rough duct, high levels of turbulence intensities are also observed near the side smooth wall as well as near the rough wall.

(5) While the distribution of $\overline{u_1u_2}$ in the rough duct is qualitatively similar to that in the smooth duct, the contours of $\overline{u_1u_3}$ have extremely different features. Values of $\overline{u_1u_3}$ near the rough wall are about three times as large as those in the smooth duct. Moreover, there is not a region of closed contours enclosed by a contour for $\overline{u_1u_3}=0$ in the $\overline{u_1u_3}$ distribution of the rough duct. The qualitative features of shear stress distributions, such as existence or non-existence of closed contours, can be estimated properly from the distribution of mean rate of strain.

(6) In the rough duct, in terms of the generation of the secondary flow vortices, the contribution of the turbulent shear stress $\overline{u_2u_3}$ is almost the same as that of the anisotropy of cross-planar normal stresses $(\overline{u_2^2}-\overline{u_3^2})$. Accordingly, the convection term of the vorticity transport equation is almost balanced with the sum of the two production terms $\partial^2(\overline{u_2^2}-\overline{u_3^2})/\partial X_2\partial X_3$ and $(\partial^2/\partial X_3^2-\partial^2/\partial X_2^2)\overline{u_2u_3}$.

Acknowledgments

The authors express their appreciation to Mr. S. Nishigaki for his assistance in conducting the experiments and in reduction of the results.

References

1) Prandtl, L., *Führer durch die Strömungslehre,* pp. 207–212, Vieweg, Brauschweig, 1965.
2) Gessner, F. B. (Evaluator), "Corner Flow (Secondary Flow of the Second Kind)," *Proc. 1980-AFOSR-HTTM-Stanford Conf. Complex Turbulent Flows,* 1981, Vol. 1, pp. 182–212.
3) Nakayama, A., and Chow, W. L., "Turbulent Flows within Straight Ducts," *Encyclopedia of Fluid Mechanics,* 1986, Vol. 1, pp. 638–674.
4) Brundrett, E., and Burroughs, P. R., "The Temperature Inner-Law and Heat Transfer for Turbulent Air Flow in a Vertical Square Duct," *Int. J. Heat Mass Trans.,* 1967, Vol. 10, pp. 1133–1142.
5) Launder, B. E., and Ying, W. M., "Prediction of Flow and Heat Transfer in Ducts of Square Cross-Section," *Proc. Inst. Mech. Engrs,* 1973, Vol. 187, pp. 455–461.
6) Emery, A. F., Neighbors, P. K., and Gessner, F. B., "The Numerical Prediction of Developing Turbulent Flow and Heat Transfer in a Square Duct," *Trans. ASME, J. Heat Transfer,* 1980, Vol. 102, pp. 51–56.
7) Brundrett, E., and Baines, W. D., "The Production and Diffusion of Vorticity in Duct Flow," *J. Fluid Mech.,* 1964, Vol. 19, pp. 375–394.
8) Perkins, H. J., "The Formation of Streamwise Vorticity in Turbulent Flow," *J. Fluid Mech.,* 1970, Vol. 44, pp. 721–740.
9) Gessner, F. B., "The Origin of Secondary Flow in Turbulent Flow along a Corner," *J. Fluid Mech.,* 1973, Vol. 58, pp. 1–25.
10) Melling, A., and Whitelaw, J. H., "Turbulent Flow in a Rectangular Duct," *J. Fluid Mech.,* 1976, Vol. 78, pp. 289–315.
11) Gessner, F. B., Po, J. K., and Emery, A. F., "Measurement of Developing Turbulent Flow in a Square Duct," in *Turbulent Shear Flows 1,* ed. Bradbury, J. S., et al., pp. 119–136, Springer-Verlag, Berlin, 1979.
12) Nakayama, A., Chow, W. L., and Sharma, D., "Three-Dimensional Developing Turbulent Flow in a Square Duct," *Bull. Japan Soc. Mech. Eng.,* 1984, Vol. 27, pp. 1438–1445.
13) Fujita, H., "Turbulent Flow in Square Ducts Consisting of Smooth and Rough Planes," *Research Reports of the Faculty of Engineering, Mie University,* 1978, Vol. 3, pp. 11–25.
14) Launder, B. E., and Ying, W. M., "Secondary Flows in Ducts of Square Cross-Section," *J. Fluid Mech.,* 1972, Vol. 54, pp. 289–295.
15) Hinze, J. O., "Experimental Investigation of Secondary Currents in the Turbulent Flow Through a Straight Conduit," *Appl. Sci. Res.,* 1973, Vol. 28, pp. 453–465.
16) Humphrey, J. A. C., and Whitelaw, J. H., "Turbulent Flow in a Duct with Roughness," in *Turbulent Shear Flows 2,* ed. Bradbury, J. S., et al., pp. 174–188, Springer-Verlag, Berlin, 1980.
17) Fujita, H., Yokosawa, H., Hirota, M., and Nagata, C., "Fully Developed Turbulent Flow and Heat Transfer in a Square Duct with Two Roughened Facing Walls," *Chem. Eng. Comm.,* 1988, Vol. 74, pp. 95–110.
18) Fujita, H., Yokosawa, H., and Hirota, M., "Secondary Flow of the Second Kind in Rectangular Ducts with One Rough Wall," *Experimental Thermal and Fluid Science,* 1989, Vol. 2, pp. 72–80.
19) Yokosawa, H., Fujita, H., Hirota, M., and Iwata, S., "Measurement of Turbulent Flow in a Square Duct with Roughened Walls on Two Opposite Sides," *Int. J. Heat and Fluid Flow,* 1989, Vol. 10, pp. 125–130.
20) Hirota, M., Fujita, H., and Yokosawa, H., "Influences of Velocity Gradient on Hot-Wire Anemometry with an X-wire Probe," *J. Phys. E: Sci. Instrum.,* 1988, Vol. 21, pp. 1077–1084.
21) Patel, V. C., "Calibration of the Preston Tube and Limitations on its Use in Pressure Gradient," *J. Fluid Mech.,* 1965, Vol. 23, pp. 185–208.
22) Yavuzkurt, S., "A Guide to Uncertainty Analysis of Hot-Wire Data," *Trans. ASME, J. Fluids Eng.,* 1984, Vol. 106, pp. 181–186.
23) Hinze, J. O., *Turbulence,* 2nd ed., p. 372, McGraw-Hill, New York, 1975.
24) Nezu, I., and Nakagawa, H., "Celluar Secondary Currents in Straight Conduit," 106, 181–186. *ASCE J. Hydraulic Eng.,* 1984, Vol. 110, pp. 173–193.